The underlying cause of the increasing performance gap between loop arrays and the ultimate SNR with increasing field strength

Riccardo Lattanzi[1,2], Manushka Vaidya[1,2], Graham C Wiggins[1], and Daniel K Sodickson[1,2]

[1]*The Bernard and Irene Schwartz Center for Biomedical Imaging, Radiology, New York University Langone Medical Center, New York, NY, United States,* [2]*The Sackler Institute of Graduate Biomedical Sciences, New York University School of Medicine, New York, NY, United States*

Introduction: It has been shown that arrays of loops radiofrequency (RF) coils are near optimal for imaging the central region of a spherical object [1,2]. This was confirmed graphically in recent years using electrodynamic simulations employing a current mode expansion and dyadic Green's functions (DGF) [3-5]. These studies showed that ideal current patterns corresponding to ultimate intrinsic signal-to-noise ratio (UISNR) for a voxel near the center of a dielectric sphere do indeed form two large distributed loops, centered on the x-y plane ($\varphi = 90°$) and separated by 180 degrees in the azimuthal direction, which rotate in the same sense about an axis that precesses around the direction of the main magnetic field (z). Although it was reported that the same current patterns are ideal at any field strength, another study showed that the performance of the same array of loop coils with respect to the UISNR decreases at higher field strengths [2]. The aim of this work is to investigate why loops become less SNR efficient at high field.

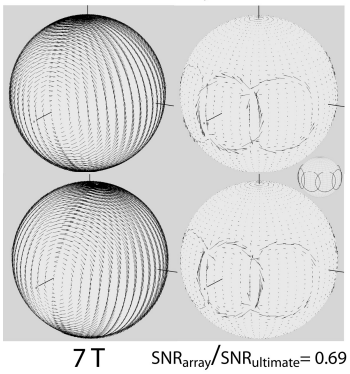

Fig. 1. A snapshot at $t = 0$ of ideal surface current patterns (left column) and current pattern for an 8-element array of loops (right column), associated with UISNR and optimal SNR in the center of sphere, respectively. Although the only difference between 1.5 T (top row) and 7 T (bottom row) is a 180 degrees phase shift, the performance of the array changes.

$$\mathbf{K}_{l,m}(\theta,\varphi) = -i\sqrt{l(l+1)}\left[W_{l,m}^{(M)}\mathbf{X}_{l,m}(\theta,\varphi) + W_{l,m}^{(E)}\hat{\mathbf{r}}\times\mathbf{X}_{l,m}(\theta,\varphi)\right] \quad (1)$$

$$\mathcal{B}_x(\mathbf{r}) - i\mathcal{B}_y(\mathbf{r}) = i\mu_0\sum_{l=0}^{+\infty}\sum_{m=-l}^{+l}\mathbf{W}^{\mathrm{T}}\mathbf{T}\begin{pmatrix}\mathbf{N}_{l,m}(k,\mathbf{r})_x - i\mathbf{N}_{l,m}(k,\mathbf{r})_y\\ \mathbf{M}_{l,m}(k,\mathbf{r})_x - i\mathbf{M}_{l,m}(k,\mathbf{r})_y\end{pmatrix} = \sum_{l=0}^{+\infty}\sum_{m=-l}^{+l}\mathbf{W}^{\mathrm{T}}\mathbf{T}\mathbf{S}(\mathbf{r}) \quad (2)$$

$$\mathbf{M}_{l,m}(\mathbf{r},k) = j_l(kr)\mathbf{X}_{l,m}(\theta,\varphi)$$
$$\mathbf{N}_{l,m}(\mathbf{r},k) = (1/k)\nabla\times\mathbf{M}_{l,m}(\mathbf{r},k) \quad (3)$$

$$\mathbf{R} = \sigma\iiint_V \mathcal{E}(\mathbf{r})\cdot\mathcal{E}^*(\mathbf{r})dV = \sum_{l=0}^{+\infty}\sum_{m=-l}^{+l}\mathbf{W}^{\mathrm{T}}\Psi\mathbf{W}^* \quad (4)$$

$$\tilde{\zeta}(\mathbf{r}_0) \sim \frac{\omega_0 M_0}{\sqrt{4k_B T_S\cdot\left(\mathbf{S}(\mathbf{r})^H\Psi^{-1}\mathbf{S}(\mathbf{r})\right)_{0,0}^{-1}}} \quad (5)$$

Theory and Methods: Given a complete basis set of current modes $\mathbf{K}_{l,m}$ (see Eq. 1) defined on a spherical surface of radius b, the resulting electric (E) field inside a dielectric sphere of radius $a<b$ can be calculated as $\mathcal{E}(\mathbf{r}) = i\omega\mu_0\int_A \bar{\mathbf{G}}(\mathbf{r},\mathbf{r}')\cdot\mathbf{K}(\mathbf{r}')dA'$ [5]. In these expressions, i is the imaginary unit, l, m are the expansion indices, $\mathbf{X}_{l,m}$ is a vector spherical harmonic of order (l, m), ω is the angular frequency, μ_o is the magnetic permeability in free space, $\bar{\mathbf{G}}(\mathbf{r},\mathbf{r}')$ is the branch of the DGF corresponding to the region indicated by $\mathbf{r}$, and $W_{l,m}^{(M)}$ and $W_{l,m}^{(E)}$ are the series expansion coefficients representing divergence-free and curl-free surface current contributions, respectively. The left circularly polarized component of the magnetic field (B) can be derived from E using Maxwell's equations and, defining $\mathbf{W}^{\mathrm{T}} = [W_{l,m}^{(M)}\ W_{l,m}^{(E)}]$, can be written as in Eq. 2, where $\mathbf{T}$ is a transformation matrix [3,4] that accounts for boundary conditions at the surface of the sphere and $\mathbf{S}$ is a matrix that contains the complex signal sensitivities associated with each mode. The vector wave functions $\mathbf{M}_{l,m}$ and $\mathbf{N}_{l,m}$ are defined in Eq. 3, where k is the complex wave number and j_l is a spherical Bessel function of order l. Note that $\mathbf{T}$ is diagonal, so the divergence-free component of the signal sensitivity depends only on $\mathbf{N}_{l,m}$ and the curl-free component only on $\mathbf{M}_{l,m}$. Vector spherical harmonics are orthogonal in a spherical object, so the modes' noise covariance matrix $\mathbf{\Psi}$ associated with the noise equivalent resistance $\mathbf{R}$ (Eq. 4) is diagonal. The UISNR at any position $\mathbf{r}_0$ inside the sphere can be calculated as in Eq. 5 [1], where M_0 is the equilibrium magnetization, ω_0 is the Larmor frequency, k_B is Boltzmann's constant, and T_S is the absolute temperature of the sample. The "0,0" subscript indicates the diagonal element corresponding to target position $\mathbf{r}_0$. Ideal current patterns [3,4] are derived by performing a weighted sum of the individual current modes $\mathbf{K}_{l,m}$ using the optimal image reconstruction weights ($\mathbf{W}^{\mathrm{opt}} = (\mathbf{S}^{\mathrm{H}}\mathbf{\Psi}^{-1}\mathbf{S})\ \mathbf{S}^{\mathrm{H}}\mathbf{\Psi}^{-1}$) resulting in UISNR [1]. SNR of any actual coil can be simulated with the same formalism by applying appropriate weighting functions to the general current distribution [4,5] to model the coil current patterns. We simulated an array of 8 loops symmetrically arranged around the equator of the object. Calculations were performed using 7,442 modes ($l_{max} = 60$) for a 10 cm radius sphere with uniform electrical properties approximating average values in the human head [2]. The current distribution was defined at a distance of 5 mm from the surface of the objects.

Results and Discussion: Fig. 1 shows that, for a voxel at the center of a sphere, ideal current patterns are the same for 1.5 T and 7 T, aside from a 180° phase shift. However, the SNR of the array with respect to the UISNR is lower in the second case. Solving Eq. 2 for $\boldsymbol{r} = 0$ demonstrates that, independent of field strength, only 2 divergence-free modes ($l = 1$, $m = \pm 1$) contribute to the signal and all others are zero. From Eq. 5, we note that, although $\mathbf{\Psi}$ is calculated with a volume integral and therefore all modes contribute to it, only the 2 elements of $\mathbf{\Psi}$ multiplied by the 2 non-zero elements of $\mathbf{S}$ contribute to the noise in the UISNR. In the case of the array, the individual coils' sensitivities are weighted combinations of the 2 modes that survive in the center, but they multiply a noise covariance matrix that is not diagonal and whose elements are weighted combinations of all the divergence-free elements of $\mathbf{\Psi}$. In other words, for a voxel in the center only 2 modes contribute to the array's signal, but many modes (3,721 in our example) contribute to the noise. This explains why the array's SNR is lower compared to UISNR, but not why the performance decreases at higher field strengths. Fig. 2 shows that the divergence-free elements of $\mathbf{\Psi}$ scale differently with field strength for modes with a different value of the expansion coefficient l, due to the varying E field distribution in the dielectric object. This means that elements of the array's noise covariance matrix will scale differently between 1.5 T and 7 T. On the other hand, the coils' sensitivities will scale equally for each array element as they are generated from only 2 modes, which share the same value of l. As a result, only the signal scales equally with field strength for the ultimate and the array case, explaining why the ratio SNR_{array}/UISNR changes. Our results showed that the decreased performance at high-field in the center of the sphere is not due to the increased contribution to the UISNR of curl-free (i.e. electric-dipole type) current modes, which could not be captured by loops. However, note that for a voxel at a distance from the center, as observed in previous studies [3,4] and shown in Fig. 3, electric dipoles do contribute significantly to the shape of the ideal current patterns at high field, resulting in an even larger SNR performance gap between 1.5 T and 7 T.

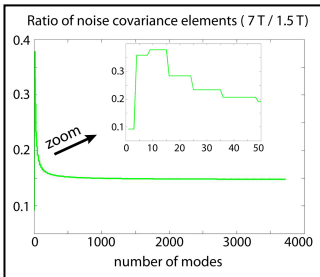

Fig. 2. The ratio of the divergence-free elements of $\mathbf{\Psi}$ at 7 T to 1.5 T is not constant, due to variations in the spatial distribution of the individual modes' electric fields.

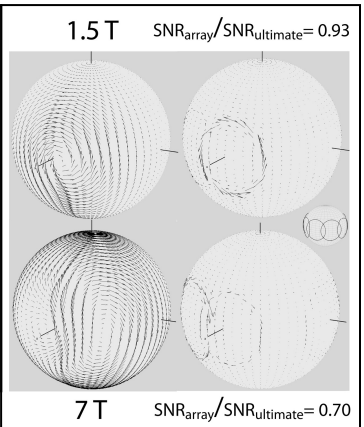

Fig. 3. Ideal surface current patterns (left column) are different at 1.5 T and 7 T for a voxel at a distance of 3 cm from the center of the sphere. The 8-element array (right column) is nearly optimal at low-field, but its performance decreases at high-field, where the contribution of the curl-free component of the current patterns becomes significant.

Conclusions: Ideal current patterns associated with UISNR in the center of a sphere take the form of large distributed loops, suggesting that arrays of loops are a reasonable choice to maximize central SNR. However, our analysis showed that discrete loops are not optimally noise-efficient, and their performance with respect to UISNR intrinsically decreases at higher field strengths.

References: [1] Lattanzi R et al. (2010) NMR Biomed 23(2):142-51 [2] Wiesinger F et al. (2005) ISMRM p.672 [3] Lattanzi R and Sodickson DK (2008) ISMRM p.78 [4] Lattanzi R and Sodickson DK (2011), ISMRM p.3876; MRM *in press.* [5] Tai CT, Dyadic Green Functions in Electromagnetic Theory (1994)